International Journal of ChemTech Research
CODEN (USA): IJCRGG ISSN: 0974-4290
Vol.8, No.10 pp 367-374, 2015

Lower leakage current through nano particles 304-L stainless steel coated with thin film

A. Ebrahimikia

Department of Solid State Physics, University of Mazandaran, Babolsar, Iran

Abstract: Layer of Ni-Fe was synthesized on stainless steel and deposited on sample with using the chemical sol-gel and dip coating routes, respectively. Nano crystallite and amorphous structures thin layers were investigated with atomic force microscopy (AFM), energy dispersive x- ray (EDX), scanning electron microscopy (SEM) and x-ray diffraction (XRD) techniques. The surface roughness, dielectric properties and leakage current through coated 304L- Stainless Steel (304 L- SS; a kind of SS) have been studied. The experimental results indicate that Ni plays an important role in reducing surface roughness and leakage current. Furthermore, the current measured with GPS 132A tool. The flux current sample with 20 gr Ni, synthesized at 700 °C was higher than the other present samples.
Keywords: Nano structure, Surface roughness, 304 L stainless steel, Leakage current.

Introduction

Along with experimental works that are being published and corresponding vacuum chamber designers, ultra high vacuum chamber (UHVC) experts have started to gauge the performance of current stainless steel (SS) chamber for growing ultra-pure and ultra-thin film on a suitable substrate. Researchers have reported [1-6] several experimental results which obtained with high quality ultrasonic shot peening, fiber laser and electrochemical scanning tunneling microscopy in combination with the scanning tunneling spectroscopy. They have studied local electrophysical properties, surface nanocrystallization, inter granular corrosion that determines UHVC corrosion and as-welded behavior [7,8]. Our recent work [9] is supplement by studying the surface nanocrystallization properties of extra low-carbon variation of AK steel type, show that SS sample with a 0.03 percent maximum carbon content can eliminate carbide precipitation due to welding and use in the as-welded condition, even in severe corrosive conditions [10]. It also eliminated unwanted bonds, pits and annealing elements [11].

The leakage current through the UHVC device is still too high [12]. For this purpose, UHVC coated with metallic oxide thin film has been considered as a good candidate of coated film for reducing leakage current through the SS–UHV chamber body [13-15]. Furthermore, nanocomposites composed of metal oxide nanoparticles embedded in SS matrices show magnetic, electric and catalytic properties depend on particle size [16-20].

Therefore, reduction of leakage current is a key point for fabrication of UHVC which can keep low pressure down to 10^{-14} Torr for growing, synthesizing so pure ultra- thin and nano scale materials inside UHVC. Reduced dirty and impurity can strongly change the thickness of ultra-thin film down to 1-2 nm [15]. Moreover, the vacuum chamber should also stand its stability to prevent corrosion. The present study synthesized nano Ni-Fe particles by sol-gel method and then coated 304L- SS with Ni-Fe film by dip coating method. Our results

indicate that 304L-SS with 20 gr Ni content (synthesized at 500 ^{o}C) respect with conventional SS device (mass %; 11.95 Ni) due to its less fractural structure and light atom penetration can be used for the next UHVC generations.

Experimental

The materials were used for synthesis with sol-gel: $Fe(NO_3)_3$, $9H_2O$ (Merck), $Ni(NO_3)_2$, $6H_2O$ (Merck), NaOH, $(NH_4)_2CO_3$, $6H_2O$ (Merck), ethylene glycol (p.a.), ethanol (C_2H_5OH) and tetra ethyl ortho silicate (TEOS) (Fluka,98%). The metallic nitrates with different stoichiometricratios, have been dissolved in ethylene glycol and ethanol. The obtained solution has been slowly added into ethanol, TEOS and NaOH solutions by drops while stirring. The homogenous and clear gel was obtained after 24 h stirring in at room temperature and air atmosphere. The obtained gels have been dried at 80 ºC for 15 minutes in oven. After drying and milling, the resulted powders have been annealed at different temperatures (100^{o} C – 700 ^{o} C) with 10- 30 gr Ni nano particles.

The 304 L-SS samples (3cm×1cm, 20 mm thickness) prepared by polished from one side for ensuring smooth surface into ethanol. Then 304 L-SS samples put in an ultrasonic bath for one hour and cleaned them by passing current through the samples several times.

A residual gas mass spectrometer has shown that a very low proportion (about 5 percent) of oxygen and carbon is produced with this setup. Typical pressures in the chamber during experiments into the vacuum chamber were around 5×10^{-7} Torr. The chemical compositions are recorded in Table 1.

Table1: Chemical composition of 304 L-SS (mass %).

C	Cr	Ni	Mo	Mn	Si	Cu
0.019	17.07	11.95	2.04	1.68	0.35	little

Discussion and Result

The structural evolution of samples is characterized by XRD, SEM, EDX, and AFM techniques. XRD spectra are performed with $Cu_{k\alpha}$ radiation ($\lambda = 1.5406 A^{\circ}$) source, at scan rate 1(degree/min) for 2θ ranging from 5^{o} to 70^{o} and shown in Figure 1.

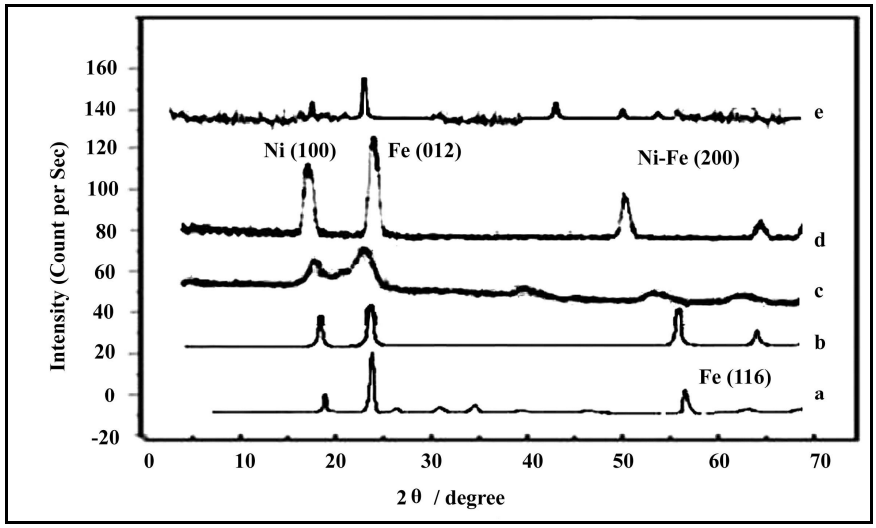

Figure 1: The XRD patterns for synthesized (a) 20 gr Ni at 100^{o} C, (b) 10 gr Ni at 500^{o} C, (c) 20 gr Ni at 500^{o} C, (d) 30 gr Ni at 500^{o} C and (e) 20 gr Ni at 700^{o} C.

Figure 1 XRD patterns shows in the crystallization structure at 100°C (with 20 gr Ni nano particles), 500°C (with 10 and 30 gr Ni nanoparticles) and 700 °C (with 20 gr Ni nano particles). The dominated peaks

exhibit the face center cubic (FCC) crystallite structures. As shown in Figure 1(c), the sample annealed at 500 °C with 20 gr Ni nano particles is nearly amorphous.

Table 2: there are Lattice parameter (a) and Brage planar distance (d_{101}) of coated layers measured for 20 gr Ni nanoparticles at different temperatures.

T(°C)	100	500	700
D(scherrer)	4.18	4.19	4.21
D(X-powder)	2.7016	3.1	3.1002

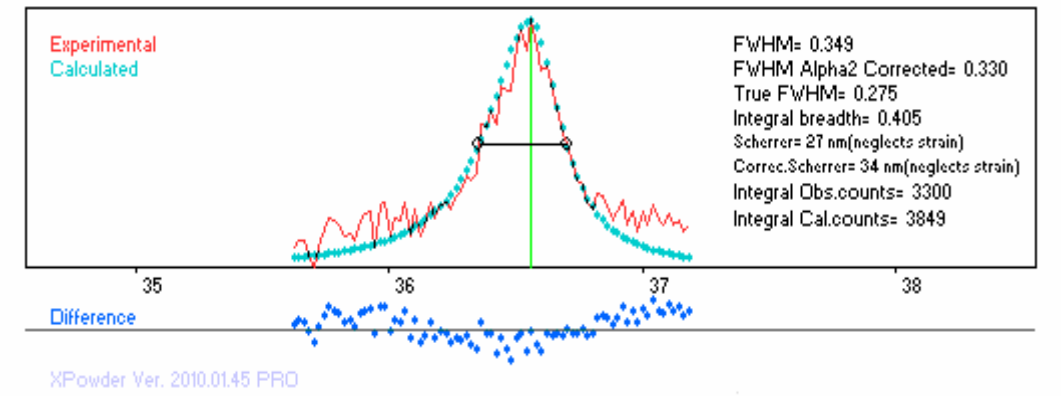

Figure 2: X- Powder software calculated Brage planar distance (d_{101}) of layer with 20 gr Ni, annealed at 700 °C.

Additionally, the Ni-Fe lattice parameter increases with increasing temperature. Figure 2 displaysd-spacing measurement for the sample with 20 gr Ni, synthesized at 700 °C. Table 2 shows that the lattice parameter (a) and Brage planar distance (d_{101}). For patterns with 20 gr Ni, and lattice parameters (d) increased with increasing temperature.

The average nanocrystallite size can be deduced from Scherer equation [1]:

$$D = \frac{K\lambda}{\beta \cos\theta} \qquad (1)$$

Where D is the crystallite size of nano crystallites, K is a constant value (0.94), λ is the wavelength of X-ray ($Cu_{k\alpha}$= 1.5406Å), β is the full width at half maximum (FWHM), and θ is the center of diffraction angle. X-powder software has also been used to measure the crystallite size (Scherer equation can be applied for spherical crystallites). The size of nano crystallite found by Scherer equation (Eq.1) and X- powder software are listed in Table 3.The layer with 20 gr Ni, synthesized at 500 °C lead to amorphous structure.

As shown in Figure 3, there are Fe-Ni sol material in the hot plate with magnet. The SS sample was immediately transformed in the hot plate and dip-coated. We could found the element of Fe, Ni, C, O and Si in the sample. By considering and focusing on Ni peak, we pursue, some difficulties which still exist in forming ideal SS (i.e., free of porosity, contamination, interstices, etc). These issues are obstacles for growing pure ultra-thin film and getting the desirable pressure inside UHVC. In fact, the majority of failures of UHVC engineering materials are very sensitive to the hug peaks of Fe, C and O in the structure and existence of the other transition peaks due to K_β and K_γ and so on beside K_α transition. Figure 3 shows low background that meaning some other transitions, inter band transitions and surface Plasmon could be remarkably reduced. It means that the better structure could be formed with 20 gr Ni nano particles at 500 °C.

The presence of Ni and O in SS matrix revealed with EDX technique (Figure 4) during synthesizing processes are responsible for these structural changes, which can lead to changes in their electrical properties as well.

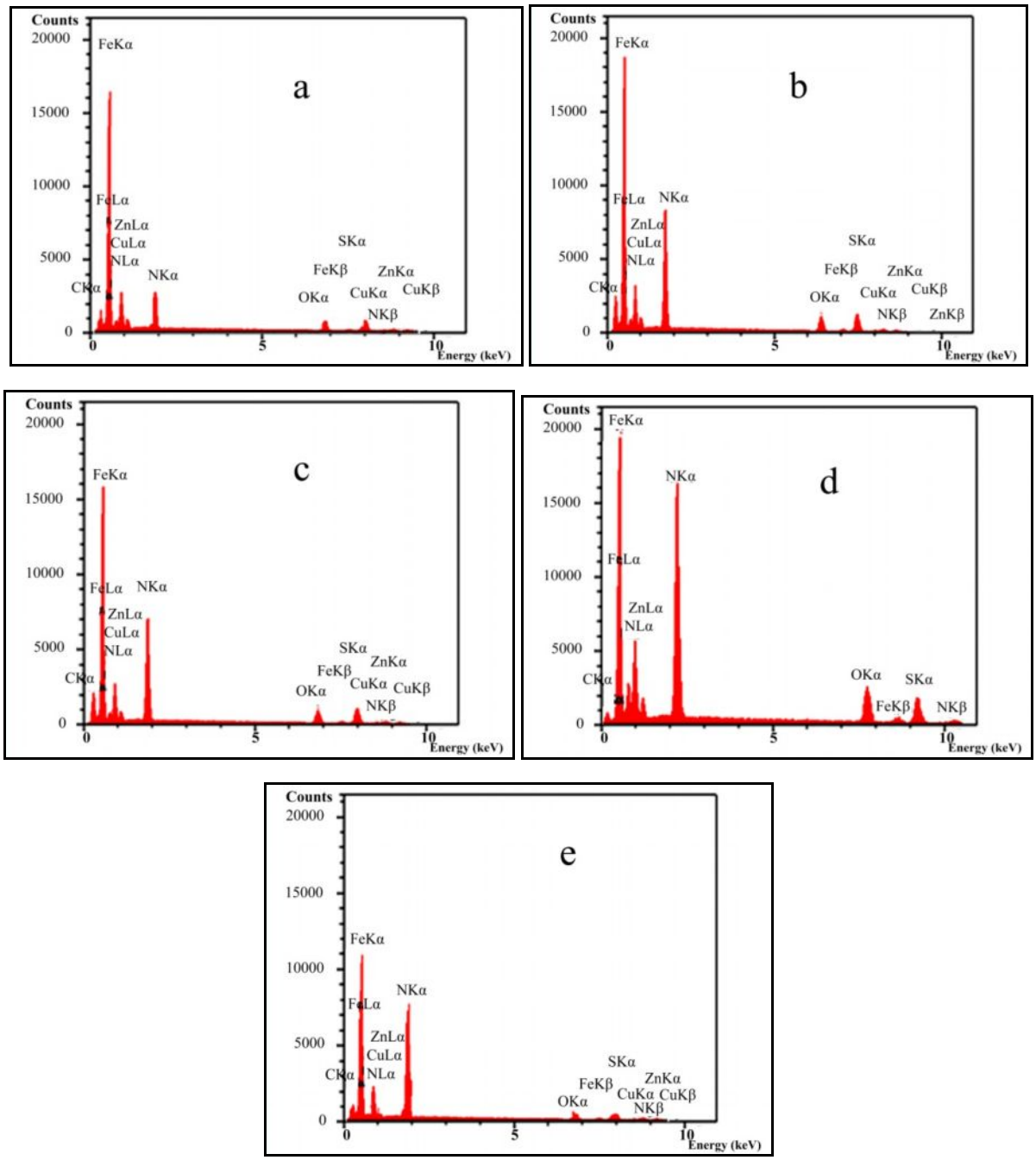

Figure 3: EDS results show wt% elements on coated 304 L stainless steel.

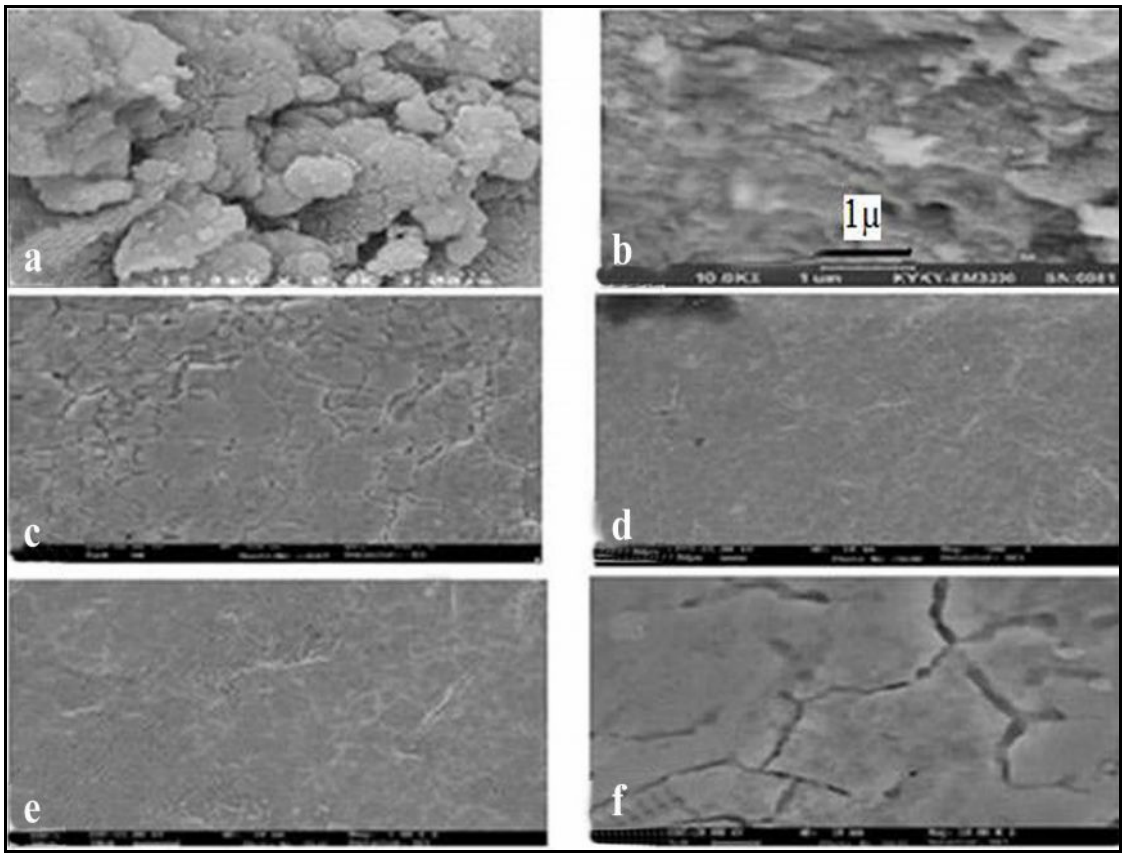

Figure 4: SEM images of 304 L SS coated with Ni-Fe synthesized (a) 10 gr Ni at 100 ° C, (b) 10 gr Ni at 500 ° C, (c) 20 gr Ni at 100° C, (d) 20 gr Ni at 500 ° C, (e) 30 gr Ni at 500 ° C.

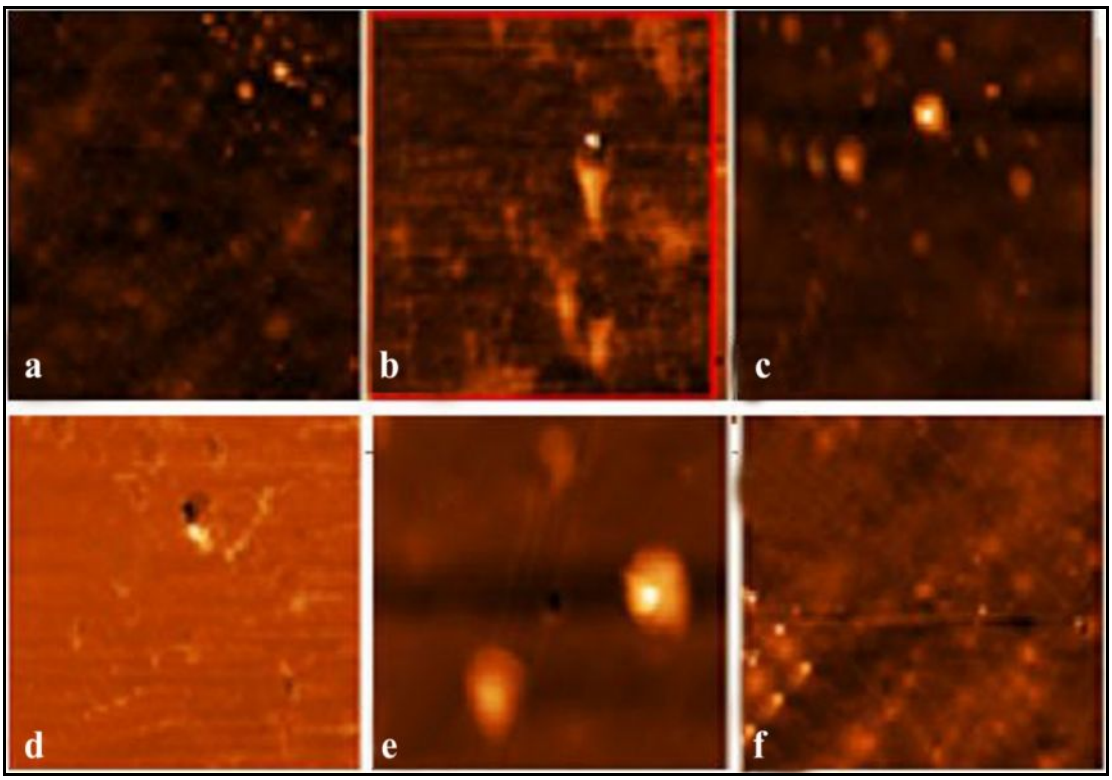

Figure 5: AFM images of 304 L SS coated with Ni-Fe synthesized (a) 10 gr Ni at 100 ° C, (b) 10 gr Ni at 500 ° C, (c) 20 gr Ni at 100 ° C, (d) 20 gr Ni at 500 ° C, (e) 30 gr Ni at 500 ° C and (f) 20 gr Ni at 700 °C.

In parallel to XRD and EDX techniques, the samples were analyzed by using SEM (Figure 4), AFM morphology and topography spectra (Figure 5).

Topography spectra and Nano surf data (Table 4) indicate AFM applications concentrate on characterizing statistical in table 4 properties of these coatings, found rather than the size of specific structures. The roughness values (The average roughness (S_a), mean value (S_m) and root mean square (Sq)) are calculated according to the following formula:

$$S_a = \frac{1}{N}\sum_{l=0}^{N-1}|z(x_l)| \quad (2)$$

$$S_m = \frac{1}{N}\sum_{l=0}^{N-1} z(x_l) \quad (3)$$

$$S_q = \sqrt{\frac{1}{N}\sum_{l=0}^{N-1}(z(x_l))^2} \quad (4)$$

The valley depth (S_v) is lowest value, the peak height (S_p) is highest value and the peak-valley height is (S_Y).

$$S_Y = S_P - S_V \quad (5)$$

Different surface roughness at 100, 500 and 700 ºC shown in Table 4, demonstrated that the sample 20 gr 500 °C has lower S_q (7.314 nm) and S_m (3.565 nm) respect with other sample present.

Table 4: Roughness parameters obtained for 304L- SS coated with Ni-Fe thin layer at different temperature.

Roughness parameter (nm)	Sample with 20 gr Ni, Synthesized at 100°C	Sample with 20 gr Ni, Synthesized at 500°	Sample with 20 gr Ni, Synthesized at 700°C
S_a	6.551	5.7110	19.013
S_q	8.632	7.314	22.584
S_y	5.384	1.218	54.152
S_m	4.861	3.565	18.018

In the present work, the pattern with 20 gr Ni annealed at 500 °C shows S_q so much decrease. Uniform surface is observed for 304 L-SS coated with 20 gr Ni at 500 °C. The SEM and AFM images exhibit crack surface morphology for 20 gr Ni synthesized at 100 °C, 10 and 30 gr Ni synthesized at 500 °C and 20 gr Ni synthesized at 700 °C. Lower roughness and crack free of the sample surface with 20 gr Ni at 500 °C (nearly amorphous structure) makes it more mechanical stable structure. Lower cracks indicate leakage flow into the chamber is reduced.

To study leakage current and/or light atom penetration through the SS coated with thin layer of Ni-Fe film with deep coating method, we used Poole–Frenkel model [16] can be written as:

$$J = AT^2 \exp\frac{1}{k_B T}\left[\left(\frac{57.7\ eV}{Kd}\right)^{1/2} - \varphi_t\right] \quad (6)$$

Where, K is the dielectric constant of the film, *d* is electrode spacing, φ_t is the depth of the trap potential leakage current and A (A=120 A/cm^{2}K^2) is the Richardson constant. . For this purpose, it is clear that T and K are key parameters. For measuring the dielectric constant we made capacitors with Ni-Fe dielectrics thin layer on 304 L-SS. By fabricating parallel plate capacitors and using LCR meter (model; GPS 132 A), the capacity (c) has been measured. Consequently the dielectric constant has been determined with using the following equation:

$$C = K\frac{A\varepsilon_0}{d} \quad (7)$$

Where C is capacitance, ε_0 ($\varepsilon_0 = 8.85 \times 10^{-12}$ ($F \cdot m^{-1}$) is the permittivity of free space, A (A = 1.2 Cm^2) is the area of the capacitor, d (d = 3 mm) is the thickness of the dielectric and film K is dielectric constant. The resulting are listed in table 5. The electrical resistivity of the films decreases with the Ni contents. As shown in Table 5 (for the sample with 10- 30 gr Ni and T= 100–700 ^oC), self-inductance (*L*), resistor (*R*), *C*, K, Quality Factor (Q_F) and Dissipation Factor (D_F) have obtained for samples with 10- 30 gr Ni and annealed at 100 ^oC – 700 ^oC temperatures.

Table 5: L, C, R, k, Q_F and D_F are measured with GPS 132 A.

Sample	L (H)	C (pF)	R(MΩ)	K	Q_F	D_F
20 gr Ni & T= 100^{o}C	18.5	9.7	2.725	27.4	0.9406	1.0632
10 gr Ni & T= 500^{o}C	205.3	10.2	2.673	28.8	1.2320	0.4480
20 gr Ni & T= 500^{o}C	361.6	13.8	3.216	38.9	2.2320	0.6172
30 gr Ni & T= 500^{o}C	270.1	12.7	2.710	35.6	1.6070	0.6222
20 gr Ni & T= 700^{o}C	190.9	11.3	2.161	31.9	1.6200	0.8117

Table 6: Current flux (I) through the capacitor versus applied voltage (V= 0.15 KV).

Sample	20 gr Ni, T= 100 ^{o}C	10 gr Ni, T= 500 ^{o}C	20 gr Ni, T= 500 ^{o}C	30 gr Ni, T= 500 ^{o}C	20 gr Ni, T= 700 ^{o}C
I (mA/m^2)	0.11	0.09	0.06	0.1	0.15

Different k values show that coated Ni-Fe samples with 20 gr Ni at 500 ^oC, has higher dielectric constant. To test the samples, we found the rate of energy less the quality factor (a_f) and the sample tunneling, higher quality factor due to dipole moments amplification.

$$Q_F = 2\pi \times \frac{\text{EnergyStored}}{\text{Energydissipatedper cycle}} \qquad (8)$$

D_F is rate of energy loss in capacitor as follow

$$D_F = \frac{1}{Q_F} \qquad (9)$$

Higher Q_F indicates a lower rate of energy loss relative to the stored energy in capacitor.

D_F can vary depending on Ni crystallite size, the dielectric material and synthesized temperature. Increased temperature and decreased $\mathbf{D_F}$ observed with increase Ni content.

Surface morphology of Ni-Fe thin layer on 304L- SS are characterized by EDX, SEM, XRD, AFM techniques. The effect of Ni content and temperatures on 304L- SS synthesized the formation of Ni-Fe coated layer lead to change leakage current the structure. Results indicate that the 20 gr Ni content in thin film layer strongly influences the phase's formation, lower leakage current, more stable structure and homogeneous distribution of the thin film layer that can be used for the future of UHVC productions.

References:

1. Bahari A, Robenhagen U, Morgen P, Li ZS. Growth of ultrathin silicon nitride on Si (111) at low temperatures. Physical Review B., 2005, 72; 205323.
2. Bahari A, Morgen P, Pedersen K, Li ZS. Growth of a stacked silicon nitride/silicon oxide dielectric on Si (100). Journal of Vacuum Science & Technology B., 2006, 24; 2119.
3. Chandra A. Synthesis and ion transport characterization of hot-pressed Ag+ ion conducting glass-polymer electrolytes. Indian Journal of Physics., 2013, 87; 643.
4. Shahmiri MR, Bahari A, Karimi-Maleh H, Hosseinzadeh R, Mirnia N. Ethynylferrocene–NiO/MWCNT nanocomposite modified carbon paste electrode as a novel voltammetric sensor for simultaneous determination of glutathione and acetaminophen. Sensors and Actuators B: Chemical., 2013, 177; 70.

5. Gutiérrez A, Domínguez-Cañizares G, Jiménez JA, Preda I, Díaz-Fernández D, Jiménez-Villacorta F, Soriano L. Hexagonally-arranged-nanoporous and continuous NiO films with varying electrical conductivity. Applied Surface Science., 2013, 276; 832.
6. Tahmasbpour B, Bahari A, Hashemizadeh SA. Synthesize and Investigate the Austenitic Nanostructural Propertise., 2012, S2; 169.
7. Kadry S. Corrosion analysis of stainless steel. Eur. J. Sci. Res., 2008, 22; 508.
8. Heilmann P, Don J, Sun TC, Rigney DA, Glaeser WA. Sliding wear and transfer. Wear., 1983, 91; 171.
9. Hineman MA, Danko MJ, Schmidt FE. An Unusual Corrosion Condition in Welded Stainless Steel Pipes. Microscopy and Microanalysis., 2012, 18; 1762.
10. Morgen P, Bahari A, Pedersen K. Nanostructured Films on Silicon Surfaces. In Functional Properties of nanostructured Materials. Springer Netherlands., 2006, 233; 229.
11. Ushijima K, Yamada Y, Yano TT, Tashiro M. An electrosurgical burn possibly caused by radio-frequency leakage current through a stainless forceps. Masui., 2000, 49; 909.
12. Weng LW, Uen WY, Lan SM, Liao SM, Yang TN, Wu CH, Shen CC. Characterizations of arsenic-doped zinc oxide films produced by atmospheric metal-organic chemical vapor deposition. Applied Surface Science., 2013, 277; 1.
13. Chong KP, Garboczi EJ. Smart and designer structural material systems. Progress in Structural Engineering and Materials., 2002, 4; 417.
14. Chong KP. Nanoscience and engineering in mechanics and materials. Journal of Physics and Chemistry of Solids., 2004, 65; 1501.
15. Bahari A, Gholipur R. Electrical and optical properties of ZrxLa1− xOy nanocrystallites as an advanced dielectric for the next FET devices. Journal of Materials Science: Materials in Electronics., 2013, 24; 674.
16. Zou DG, Liu R, Li J, Zhang W, Wang D, Han Y. Corrosion Resistance and Semiconducting Properties of Passive Films Formed on 00Cr13Ni5Mo2 Supermartensitic Stainless Steel in Cl− Environment. J. Iron.Steel.Res., 2014, 21; 630.
17. Zou DG, Liu XH, Han Y, Zhang W, Li J, Wu K. Influence of Heat Treatment Temperature on Microstructure and Property of 00Crl3Ni5Mo2 Supermartensitic Stainless Steel. J. Iron.Steel.Res., 2014, 21; 364.
18. Yue W, Zhou W. Porous crystals of cubic metal oxides templated by cage-containing mesoporous silica. Journal of Materials Chemistry., 2007, 17; 4947.
19. Balachandran R, Yow HK, Ong BH, Tan KB, Anuar K, Wong HY. Surface morphology and electrical properties of pulse electrodeposition of Ni-Fe films on copper substrates in ultrasonic field. Int. J. Electrochem. Sci., 2011, 6; 3564.
20. Liu X, Yu WG, Zhang QF, Jiang SM. Influence of Surface Roughness of Galvanized Steel Sheet on Self-lubricated Coating. J. Iron.Steel.Res., 2014, 21; 342.

*****